JEM Journal of Experimental Medicine

ARTICLE

Resident memory CD8 T cells persist for years in human small intestine

Raquel Bartolomé-Casado[1], Ole J.B. Landsverk[1], Sudhir Kumar Chauhan[1,2], Lisa Richter[1,3], Danh Phung[1], Victor Greiff[4], Louise F. Risnes[5,6], Ying Yao[4,6], Ralf S. Neumann[4,6], Sheraz Yaqub[7], Ole Øyen[8], Rune Horneland[8], Einar Martin Aandahl[2,8], Vemund Paulsen[9], Ludvig M. Sollid[4,5,6], Shuo-Wang Qiao[4,6], Espen S. Baekkevold[1], and Frode L. Jahnsen[1]

Resident memory CD8 T (Trm) cells have been shown to provide effective protective responses in the small intestine (SI) in mice. A better understanding of the generation and persistence of SI CD8 Trm cells in humans may have implications for intestinal immune-mediated diseases and vaccine development. Analyzing normal and transplanted human SI, we demonstrated that the majority of SI CD8 T cells were bona fide CD8 Trm cells that survived for >1 yr in the graft. Intraepithelial and lamina propria CD8 Trm cells showed a high clonal overlap and a repertoire dominated by expanded clones, conserved both spatially in the intestine and over time. Functionally, lamina propria CD8 Trm cells were potent cytokine producers, exhibiting a polyfunctional (IFN-γ$^+$ IL-2$^+$ TNF-α$^+$) profile, and efficiently expressed cytotoxic mediators after stimulation. These results suggest that SI CD8 Trm cells could be relevant targets for future oral vaccines and therapeutic strategies for gut disorders.

Introduction

Studies in mice have shown that the intestine contains high numbers of resident memory CD8 T (Trm) cells (Steinert et al., 2015). CD8 Trm cells are persistent, noncirculatory cells that provide particularly rapid and efficient protection against recurrent infections (Ariotti et al., 2014). In addition to their cytotoxic activity, CD8 Trm cells are efficient producers of proinflammatory cytokines that rapidly trigger both innate and adaptive protective immune responses (Schenkel et al., 2014). Thus, CD8 Trm cells are attractive targets for vaccine development against intracellular pathogens (Gola et al., 2018) and cancer immunotherapy (Park et al., 2019).

Although studies in mice have significantly advanced our understanding of CD8 Trm cell function in the intestine (Jabri and Ebert, 2007; Sheridan et al., 2014; Konjar et al., 2018), translation of mouse data into humans should be implemented with caution. Specifically, the generation of T cell memory in humans occurs after exposure to a broad variety of pathogens and commensals over many decades of life, which cannot be recapitulated in mouse models. Most mice are maintained in specific pathogen–free conditions that reduce their microbiome diversity, which in turn influences the immune homeostasis and response to pathogens in the intestine (Maynard et al., 2012; Tao and Reese, 2017). Moreover, murine intraepithelial (IE) CD8 T cells constitute a heterogeneous population of unconventional CD8αα$^+$ and conventional CD8αβ$^+$ T cells, with partially overlapping effector properties but different developmental origins (McDonald et al., 2018). In contrast, their human counterparts mainly consist of conventional CD8αβ-expressing cells (Jabri and Ebert, 2007).

Under steady state conditions, the human small intestine (SI) is densely populated by CD8 T cells, in both the lamina propria (LP) and the epithelium. However, most studies of human SI CD8 T cells have focused exclusively on IE CD8 T cells (Abadie et al., 2012). Therefore, there is currently very limited knowledge about several functional aspects of SI CD8 T cells. For example, is the CD8 T cell population heterogeneous? Are the CD8 T cells persistent or circulating cells? What are their cytotoxic and cytokine-producing capacity? To what extent are LP and IE CD8 T cells clonally related? To consider using SI CD8 T cells as targets to design effective oral vaccines and to understand

[1]Department of Pathology, Oslo University Hospital and University of Oslo, Oslo, Norway; [2]Department of Cancer Immunology, Institute for Cancer Research, Oslo University Hospital, Oslo, Norway; [3]Core Facility Flow Cytometry, Biomedical Center, Ludwig-Maximilians-University Munich, Munich, Germany; [4]Department of Immunology, Institute of Clinical Medicine, University of Oslo, Oslo, Norway; [5]Department of Immunology, Oslo University Hospital, Rikshospitalet, Oslo, Norway; [6]K.G. Jebsen Coeliac Disease Research Centre, University of Oslo, Oslo, Norway; [7]Department of Gastrointestinal Surgery, Oslo University Hospital, Rikshospitalet, Oslo, Norway; [8]Department of Transplantation Medicine, Section for Transplant Surgery, Oslo University Hospital, Rikshospitalet, Oslo, Norway; [9]Department of Gastroenterology, Oslo University Hospital, Rikshospitalet, Oslo, Norway.

Correspondence to Raquel Bartolomé-Casado: r.b.casado@medisin.uio.no; Frode L. Jahnsen: f.l.jahnsen@medisin.uio.no.

their involvement in immune-mediated diseases, these are critical questions to address.

Analyzing the CD8 T cell compartment in the normal SI as well as in a unique transplantation setting in humans, we report that most SI CD8 T cells are Trm cells that persist for >1 yr in the epithelium and LP. High-throughput TCR sequencing (TCR-seq) showed a polarized immune repertoire and high clonal relatedness between IE and LP CD8 Trm cells. Functionally, the minor population of LP CD103$^-$ CD8 T cells was transient in the tissue and produced fewer cytokines but had more preformed cytotoxic granules. In contrast, we demonstrate that activated CD8 Trm cells expressed high levels of multiple cytokines (polyfunctional) and showed de novo production of cytotoxic granules. Thus, SI CD8 Trm cells have potent protective capabilities and present functional roles similar to CD8 Trm cells described in mice.

Results

Most CD8 T cells in the human SI express a resident memory phenotype

To determine whether the human SI contains persisting CD8 T cells, we first examined biopsies from donor duodenum after pancreatic-duodenal transplantation (Tx) of type I diabetic patients (Horneland et al., 2015). Using fluorescent in situ hybridization probes specific for X/Y chromosomes on tissue sections where patient and donor were of different gender, we could precisely distinguish donor and recipient cells and consistently detected a high fraction of persisting donor CD8 T cells 1 yr after Tx (Fig. 1 A).

This finding encouraged us to further characterize SI CD8 T cells, and to this end we examined resections of proximal SI obtained from pancreatic cancer surgery (Whipple procedure) and from donors and recipients during pancreatic-duodenal Tx (baseline samples). All tissue samples were evaluated by pathologists, and only histologically normal SI was included. Peripheral blood (PB) was collected from Tx recipients and pancreatic cancer patients, and PB mononuclear cells (PBMCs) were isolated and analyzed by flow cytometry together with single-cell suspensions from enzyme-digested LP and IE. The cross-contamination between IE and LP fractions was negligible, attested by complete removal of epithelial cells assessed by histology (Fig. S1 A) and by low numbers of epithelial cells in the LP fraction detected by flow cytometry (Fig. S1 B). We found that, in blood and SI-LP, CD8 T cells constituted about a third of the CD3 T cells, while CD8 T cells dominated (>75%) in the epithelium (Fig. S1 C). Almost all SI CD8 T cells were TCRαβ$^+$ (≈99.8% in LP and 98.7% in epithelium; Fig. S1 D), and virtually all expressed the coreceptor CD8αβ (Fig. S1 E). The vast majority of SI CD8 T cells exhibited a CD45RO$^+$ CD45RA$^-$ L-Sel$^-$ CCR7$^-$ effector memory phenotype (Fig. 1 B), whereas PB also contained a substantial fraction of naive (CD45RO$^-$ CD45RA$^+$ CCR7$^+$ L-Sel$^+$) and central memory (CD45RO$^+$ CD45RA$^-$ CCR7$^+$ L-Sel$^+$) CD8 T cells (Fig. 1 B).

To further define and compare LP and IE CD8 T cells with PB CD8 T cells, we performed t-distributed stochastic neighbor embedding (t-SNE) analysis including classic Trm markers and functional (e.g., costimulatory and inhibitory) receptors associated with a Trm phenotype (Mackay et al., 2013; Thome et al., 2014; Fergusson et al., 2016; Kumar et al., 2017). LP and IE CD8 T cells clustered together and were distinct from PB CD8 T cells (Fig. 1 C, left). By visualizing the expression pattern for each marker, we confirmed that cells expressing CD45RA and CCR7 were confined to the PB clusters, whereas the Trm markers CD69 and CD103 were expressed only on tissue-derived CD8 T cells. SI CD8 T cells also showed high expression of the co-inhibitory receptor 2B4 (SLAMF4) and the C-type lectin natural killer receptor CD161, whereas CD28 and killer-cell lectin like receptor G1 (KLRG1) were expressed at higher levels on PB CD8 T cells. CD127 (IL7 receptor-α), NKG2D, and PD-1 did not show any clustered expression (Fig. 1 C).

Virtually all LP and IE CD8 T cells expressed CD69 (97.15% and 99.6%, respectively). CD103 was expressed by most (76%) LP CD8 T cells and by all IE CD8 T cells (Fig. 1 D), whereas the minor population of LP CD8 T cells lacking CD103 was more similar to PB CD8 T cells (Fig. 1 C). Given that CD103 is the currently most established marker to infer residency at mucosal surfaces (Beura et al., 2018b), we evaluated the phenotypic profiles of CD103$^+$ and CD103$^-$ SI CD8 T cells in a larger cohort of donors (Fig. 2 A). CD127 was expressed by a larger fraction of LP CD103$^+$ CD8 T cells than IE CD103$^+$ and LP CD103$^-$ CD8 T cells (Fig. 2 A). However, IE CD103$^+$ CD8 T cells had higher expression of 2B4 and CD161 compared with CD103$^-$ CD8 T cells. NKG2D was broadly expressed on all SI CD8 T cell subsets, but showed significantly higher expression in the CD103$^-$ compartment. In addition, we found consistently higher numbers of cells positive for CD28, PD-1, and KLRG1 within the CD103$^-$ CD8 T population compared with both LP and IE CD103$^+$ cells (Fig. 2 A). Interestingly, approximately half of the CD103$^-$ CD8 T cells expressed KLRG1, whereas most CD103$^+$ CD8 T cells were KLRG1$^-$, and plotting CD103 versus KLRG1 divided LP CD8 T cells into three distinct subsets (Fig. 2 B). The distribution of these three LP CD8 T cell subsets was conserved lengthwise in the SI, as demonstrated by their similar representation in mucosal biopsies taken several centimeters apart in the same SI (Fig. S2 B). We also analyzed the expression of the proliferation marker Ki67 by intracellular staining and flow cytometry. We detected few Ki67-positive cells (median <5%) in all CD8 T cell subsets from normal SI samples (Fig. 2 C), indicating that the proliferative activity of SI CD8 T cells under steady state conditions is low. To summarize, we showed that the majority of LP CD8 T cells and nearly all IE CD8 T cells express a Trm phenotype (CD103$^+$ KLRG1$^-$), whereas a minor fraction in the LP was more similar to PB CD8 effector memory cells, being CD103$^-$ KLRG1$^{+/-}$.

CD8 Trm cells persist for ≥1 yr in transplanted SI

Next, we wanted to determine whether CD8 T cells expressing a Trm phenotype were maintained over time in the human SI. The in vivo replacement kinetics of CD8 T cells in duodenal biopsies obtained by endoscopy was examined at 3, 6, and 52 wk after Tx (Horneland et al., 2015; for details, see Fig. S3 A). Most donors and patients express different HLA type I molecules, making it possible to accurately distinguish persisting donor cells from newly recruited incoming recipient cells in the graft by flow

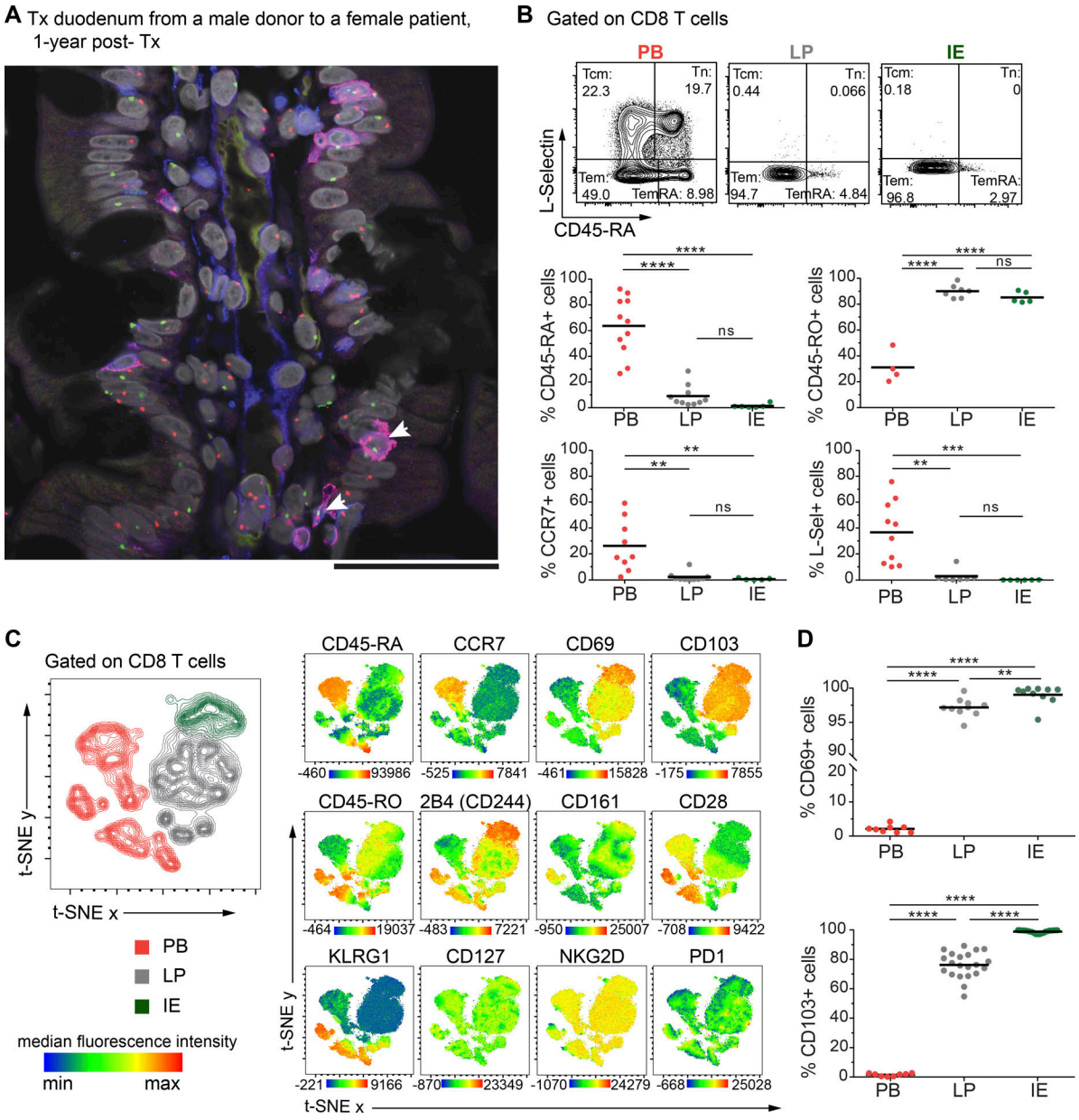

Figure 1. **Human SI mucosa harbors a substantial population of CD8 T cells with a Trm phenotype. (A)** Representative confocal image of a tissue section from a male donor duodenum 1 yr after Tx into a female patient stained with X/Y chromosome fluorescent in situ hybridization probes (Y, green; X, red) and antibodies against CD8 (red) and CD3 (blue). Hoechst (gray) stains individual nuclei, and white arrows indicate donor (male) CD8 T cells (n = 8). Scale bar, 50 µm. **(B)** Expression of classic lymph node homing and memory markers on PB, LP, and IE CD8 T cells. Representative contour plots and compiled data for each marker are given. Tcm, central memory CD8 T cell; Tem, effector memory CD8 T cell; Tn, naive CD8 T cell. **(C)** t-SNE map showing the distribution of PB (red), LP (gray), and IE (green) CD8 T cell clusters (left). Overlay of the t-SNE map with expression levels for each marker, color-coded based on the median fluorescence intensity values, representative of three samples. See Fig. S2 A for details on preprocessing of flow data for t-SNE analysis. **(D)** Compiled data for the expression of CD69 and CD103 on PB, LP, and IE CD8 T cells. Black bars in B and D indicate mean values. Statistical analysis was performed using one-way ANOVA with Tukey's multiple comparisons test. ns, not significant; **, P ≤ 0.01; ***, P ≤ 0.001; ****, P ≤ 0.0001.

cytometry (Landsverk et al., 2017; Fig. 3 A). Only patients without histological or clinical signs of rejection were included (n = 32). At 3 and 6 wk after Tx, the vast majority of LP and IE CD103⁺ CD8 T cells were still of donor origin (Fig. 3 B). Of note, on average >60% of both LP and IE CD103⁺ CD8 T cells were still of donor origin 1 yr after Tx, although there was considerable interindividual variation, with some patients showing hardly any replacement at all (Fig. 3 B).

Immunophenotyping showed that the persisting donor CD103⁺ CD8 T cells expressed a Trm phenotype similar to the baseline situation (Fig. S3 B). LP CD103⁻ CD8 T cells were more rapidly replaced by recipient CD8 T cells, and at 6 wk after Tx, only 34% of the cells were of donor origin; however, after 1 yr, the LP CD103⁻ CD8 T cell compartment still contained ~15% donor cells (Fig. 3 B).

Within the LP CD103⁻ CD8 T cell population, the percentages of donor KLRG1⁺ and KLRG1⁻ cells were highly correlated (r^2 = 0.67,

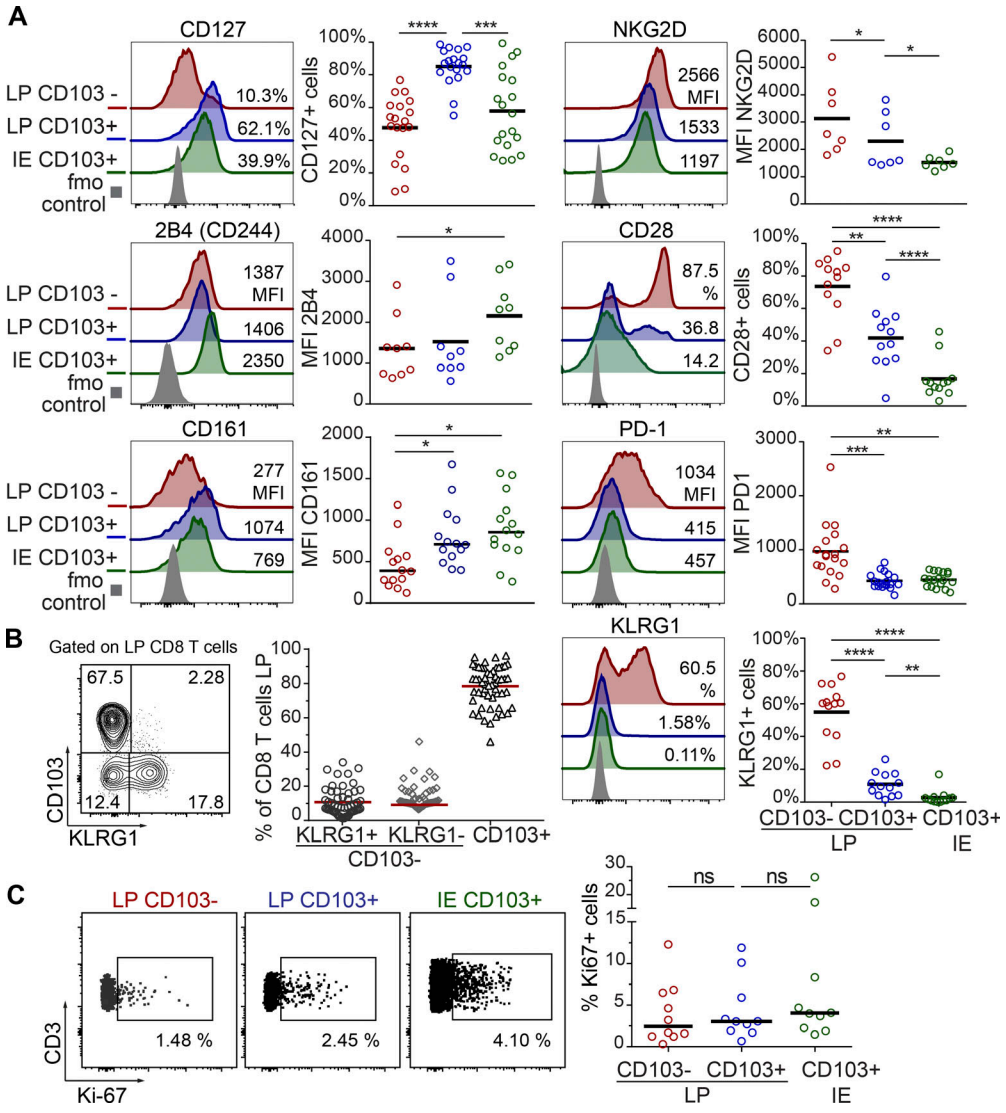

Figure 2. **LP and IE CD103⁺ CD8 T cells are phenotypically distinct from LP CD103⁻ CD8 T cells in normal human SI. (A)** Percentage of positive cells or median fluorescence intensity (MFI) values for various markers on LP CD103⁻, LP CD103⁺, and IE CD103⁺ CD8 T cells in histologically normal SI. Representative histograms for all markers are given with color codes (left): LP CD103⁻ (red), LP CD103⁺ (blue), IE CD103⁺ (green) CD8 T cells, and fluorescence minus one (fmo) control (gray). Black bars indicate mean values. **(B)** Representative contour plot (left) and fraction of LP CD103⁺ and CD103⁻ CD8 T cells expressing KLRG1 (right, *n* = 54). Red bars indicate mean values. **(C)** Representative dot plot (left) and percentage of LP CD103⁺, LP CD103⁻, and IE CD103⁺ CD8 T cells expressing Ki67 (right graph, *n* = 10). Black bars indicate median values. Statistical analysis was performed using one-way ANOVA for repeated measures with Tukey's multiple comparisons test. ns, not significant; *, P ≤ 0.05; **, P ≤ 0.01; ***, P ≤ 0.001; ****, P ≤ 0.0001.

P < 0.0001), suggesting a comparable replacement rate (Fig. 3 C). A similar replacement correlation was also found for CD103⁺ CD8 T cell subsets in LP and IE (r^2 = 0.82, P < 0.0001; Fig. S3 C). Analyzing recipient CD8 T cells, we found that 60–70% of incoming LP CD8 T cells were CD103⁻ KLRG1$^{+/-}$ at 3 and 6 wk after Tx (Fig. 3, D and E). However, 1 yr after Tx, more than half of recipient LP CD8 T cells expressed a Trm phenotype (CD103⁺ KLRG1⁻), whereas the relative fractions of CD8 T cell phenotypes were stable at all the time points in the native duodenum (Fig. 3, D and E). This suggested that incoming CD103⁻ CD8 T cells gradually differentiated into CD103⁺ Trm cells, and that the relative distribution of the CD103⁺ subset within the total recipient CD8 T cell compartment at 1 yr after Tx became similar to the steady state situation (Figs. 2 B and 3, D and E). Flow-cytometric analysis of biopsies obtained from the adjacent recipient duodenum did not show any donor-derived CD8 T cells, indicating that lateral migration or propagation from any residual lymphoid tissue in the graft was not occurring (Fig. S3 D).

To evaluate whether the surgical trauma, immunosuppressive treatment, and leukocyte chimerism was influencing the absolute numbers of SI CD8 T cells in the transplanted duodenum, we performed immunohistochemical staining of biopsies obtained at different time points from the same patients. Notably, we found that the overall density of CD8 T cells in transplanted duodenum was stable throughout the 1-yr follow-up period (Fig. S3 E). Moreover, flow-cytometric analysis of Tx tissue showed very few Ki67⁺ cells among the donor LP and IE CD103⁺ CD8 T cells (Fig. S3, F and G), similar to steady state

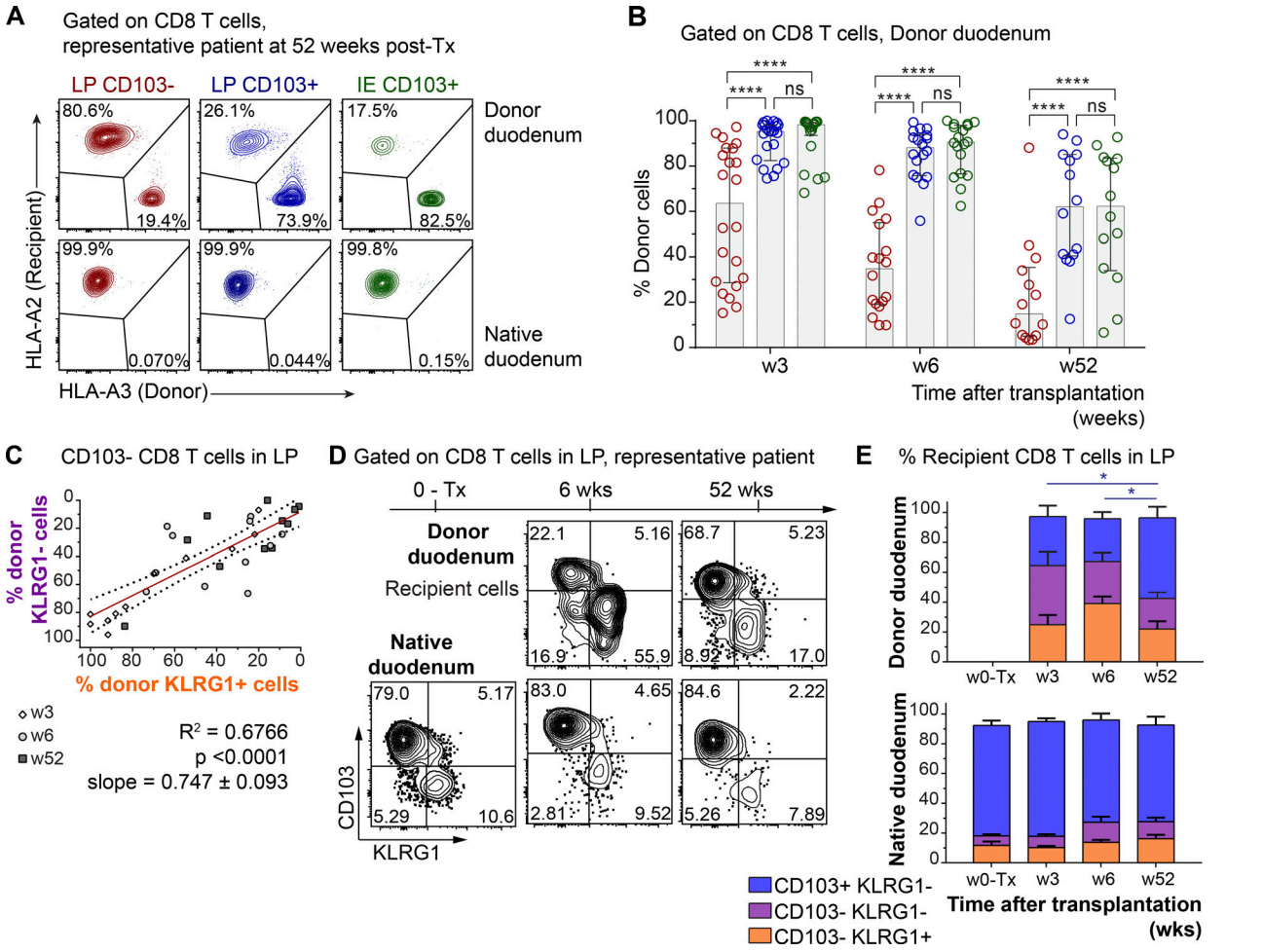

Figure 3. **CD103⁺ CD8 T cells persist for ≥1 yr, while CD103⁻ CD8 T cells are dynamically exchanged in transplanted SI. (A)** Representative contour plots showing the percentage of donor and recipient LP CD103⁺, LP CD103⁻, and IE CD103⁺ CD8 T cells in donor duodenum 52 wk after Tx (n = 14). **(B)** Percentage of donor cells in the LP CD103⁻ (left, red), LP CD103⁺ (center, blue), and IE CD103⁺ (right, green) CD8 T cell subsets at 3 (n = 21), 6 (n = 18), and 52 wk after Tx (n = 14) as determined by HLA class I expression (as in A). Gray columns indicate median values. w, week. **(C)** Pearson correlation of percentages of donor-derived cells in KLRG1⁺ and KLRG1⁻ CD103⁻ CD8 T cell subsets in LP after Tx. Statistics performed using two-tailed P value (95% confidence interval, n = 33). **(D)** Distribution of recipient-derived CD8 T cells in the LP in different subsets according to the expression of KLRG1 and CD103, in donor (top) and native duodenum (bottom), before (0-Tx) and 3, 6, and 52 wk after Tx. One representative patient sample is shown (n = 33). **(E)** Compiled data for recipient CD8 T cell subset representation in native and donor duodenum before (w0-Tx) and after (w3-52) Tx. Mean with SD is shown. Statistical analysis was performed using two-way ANOVA with repeated measures across subsets and Tukey's multiple comparisons test of CD103⁺ KLRG1⁻ subset with time. ns, not significant; *, P ≤ 0.05; ****, P ≤ 0.0001.

levels (Fig. 2 C), indicating that proliferation was not a major contributing factor to the persistence of donor T cells in transplanted intestine. Taken together, these results show that SI CD103⁺ CD8 T cells can survive for ≥1 yr in the tissue and suggest that CD103⁻ CD8 T cells recruited to the SI may differentiate into Trm cells in situ.

Single-cell TCR repertoire analysis supports long-term persistence of CD103⁺ CD8 T cells in transplanted intestine

To further explore and verify the long-term persistence of SI CD8 Trm cells in Tx, we studied the conservation of the immune repertoire of SI CD103⁺ CD8 T cells over time at the single-cell level. Specifically, we performed single-cell high-throughput TCR-seq of donor LP CD103⁺ CD8 T cells sorted from the grafted duodenum before and 1 yr after Tx. To determine if the degree of chimerism might affect the TCR repertoire, we included samples from one patient exhibiting high T cell replacement 1 yr after Tx (Ptx#1; 5% donor CD8 T cells) and one patient with low replacement (Ptx#2; 70% donor CD8 T cells; for sorting gating strategy, see Fig. S4 A). As a control, we also performed single-cell TCR-seq of LP CD103⁺ CD8 T cells from biopsies of the native (i.e., autologous, nontransplanted) duodenum of one patient (Ptx#2).

First, we investigated how many cells with the same clonotype (defined by identical nucleotide TCRα-β chains) were present in samples from the same individual taken before and 1 yr after Tx. Strikingly, despite the limited sampling, we detected overlapping clonotypes in biopsies obtained 1 yr apart in both transplanted and nontransplanted tissue. We found that 12% of the clonotypes identified at baseline were present 1 yr

after Tx in patient Ptx#1, whereas a 50 and 37% overlap was detected in patient Ptx#2 (donor and native duodenum, respectively; Fig. 4 A). The frequency distribution of the TCRα-β clonotypes at both time points was similar in all the paired samples, and the first 10 clones with higher clonal size (8 of 21 clonotypes and 10 of 35 clonotypes on average, at week 0 and week 52, respectively) represented approximately half of the repertoire in all the cases, indicating significant clonal expansion (Fig. 4 B). Most of the unique TCRα-β sequences were derived from relatively small clones (expressed only by one cell), whereas a higher proportion of expanded clones were found among those shared at both time points (Fig. 4 C).

In agreement with other reports (Han et al., 2014), we found that TCR-seq efficiency was consistently lower for TCRα. To analyze a larger number of cells, we therefore calculated the clonal overlap using only the TCRβ chain sequence. In all paired samples, the percentage of overlapping TCRβ clonotypes was comparable to that calculated for TCRα-β clonotypes (Fig. 4 D). Furthermore, TCRβ analysis showed that the shared clones were more expanded both at baseline and at 52 wk compared with the unique clones (Fig. 4 E). The degree of clonal overlap and the frequency of expanded clones were similar in the grafted and the native duodenum from the same patient (Ptx#2), suggesting that chimerism in the transplanted SI did not trigger an excessive allo-driven clonal expansion. This was substantiated by the finding that CD8 T cells showed low expression of the proliferation marker Ki67 (Fig. S3, F and G). Together, these results confirmed that persisting CD8 Trm cells survive for ≥1 yr in transplanted duodenum and showed that relatively few expanded clonotypes constitute a considerable fraction of the CD8 Trm repertoire.

LP and IE CD103$^+$ Trm cells present similar immune repertoire

The replacement kinetics and phenotype of CD8 T cells in transplanted SI (Figs. 3 B and S3 B) suggested that both IE and LP CD103$^+$ CD8 T cells are Trm cells, whereas CD103$^-$ KLRG1$^{+/-}$ CD8 T cells were more dynamic subsets that have the potential to differentiate into CD103$^+$ CD8 T cells (Fig. 3, D and E). To further interrogate the relationship among the SI CD8 T cell subsets, we sorted LP and IE CD103$^+$ CD8 T cells as well as KLRG1$^+$ and KLRG1$^-$ LP CD103$^-$ subsets from five SI samples. RNA was isolated, and TCRα and TCRβ genes were amplified by seminested PCR, including three cDNA replicates for each TCR chain (Fig. S4 B). Correlation of the read counts for the clonotypes found within the three molecular replicates was high (Fig. S4 D), indicating reproducibility of the TCR repertoire sequencing (Greiff et al., 2014). To determine whether different SI CD8 T cell subsets shared a common clonal origin, we calculated the percentage of overlapping clones and the Morisita–Horn similarity index for all the pairwise comparisons of both TCRα and TCRβ clonotypes. We found that the repertoire of LP and IE CD103$^+$ CD8 T cells was very similar, with a clonal overlap of 35.6 and 37.5% and Morisita–Horn indexes of 0.66 and 0.71, respectively (Fig. 5, A and B). Both CD103$^-$ CD8 T cell subsets had a relatively low degree of similarity with the CD103$^+$ subsets. However, notably, the Morisita–Horn index was 10-fold higher comparing LP and IE CD103$^+$ CD8 T cells with the KLRG1$^-$ subset than with the KLRG1$^+$ subset (Fig. 5 B).

To better understand the extent of clonal overlap within the SI CD8 T cell population, we measured overlapping clones across all the SI CD8 T cell subsets. Interestingly, we found that some clones were shared among three or even all four CD8 T cell subsets (representative sample in Fig. 5 C), suggesting that the same progenitor cell can give rise to all memory CD8 T cell subsets. We next assessed the clonal diversity for each subset by calculating the Shannon evenness index, which describes the extent to which a distribution of clonotypes is distanced from the uniform distribution, with values ranging from 0 (least diverse, clonal dominance) to 1 (highly diverse, all clones have the same frequency; Greiff et al., 2015b). We found that all four SI CD8 T cell subsets displayed relatively low evenness values (Fig. S4 F), indicating a polarized repertoire with prevalence of certain clones. Fig. 5 D shows the abundance of the 10 most expanded TCRα and TCRβ clonotypes in each sample. Notably, a few dominant clones constituted a large fraction of the total repertoire in all of the subsets (≤40% of the total reads in some cases). In line with their similarity values (Fig. 5 B), LP and IE CD103$^+$ T cells showed an analogous distribution of 10-top ranked clones in all five donors (Fig. 5 D).

To summarize, these data show that LP and IE CD103$^+$ Trm cells have a very similar TCR repertoire. In both cases, this repertoire is biased toward a few expanded clones, and it is more closely related to the LP CD103$^-$ CD8 T cell subset lacking KLRG1 expression.

Activated SI CD8 T cell subsets produce different levels of cytokines and cytotoxic mediators

CD8 T cells exert their effector functions through activation-induced cytotoxicity involving targeted secretion of perforin and granzyme-B and cytokine secretion. In the absence of stimulation, significantly more CD103$^-$ CD8 T cells expressed granzyme-B and perforin compared with LP and IE CD103$^+$ T cells (Fig. 6 A). However, after activation with anti-CD3/CD28 beads, both CD103$^-$ CD8 T cells and LP CD103$^+$ CD8 T cells significantly increased their expression of granzyme-B and perforin, although the level of perforin was still higher in the CD103$^-$ CD8 T cell subset (Fig. 6 B). Within the CD103$^-$ population, KLRG1$^+$ cells expressed higher levels of perforin after stimulation compared with KLRG1$^-$ cells (Fig. S5, A and B). Interestingly, induction of cytolytic molecules was hardly detectable in IE CD8 T cells, suggesting that TCR stimulation is not sufficient to activate their cytolytic function (Fig. 6 B).

To investigate their cytokine production profiles, SI CD8 T cell subsets were subjected to short-term stimulation with PMA and ionomycin, followed by intracellular flow-cytometric cytokine detection. Most (88%) LP CD103$^+$ CD8 T cells produced one or more of the cytokines tested, whereas 75% of the LP CD103$^-$ CD8 T cells and 45% of the IE CD8 T cells were positive (Fig. 6, C and D). LP CD103$^+$ CD8 T cells had a significantly higher proportion of dual IFN-γ$^+$ IL-2$^+$ cells and triple-producing (IFN-γ$^+$ IL-2$^+$ TNF-α$^+$) cells compared with the other subsets (Fig. 6 C). Moreover, triple-producing CD8 T cells expressed

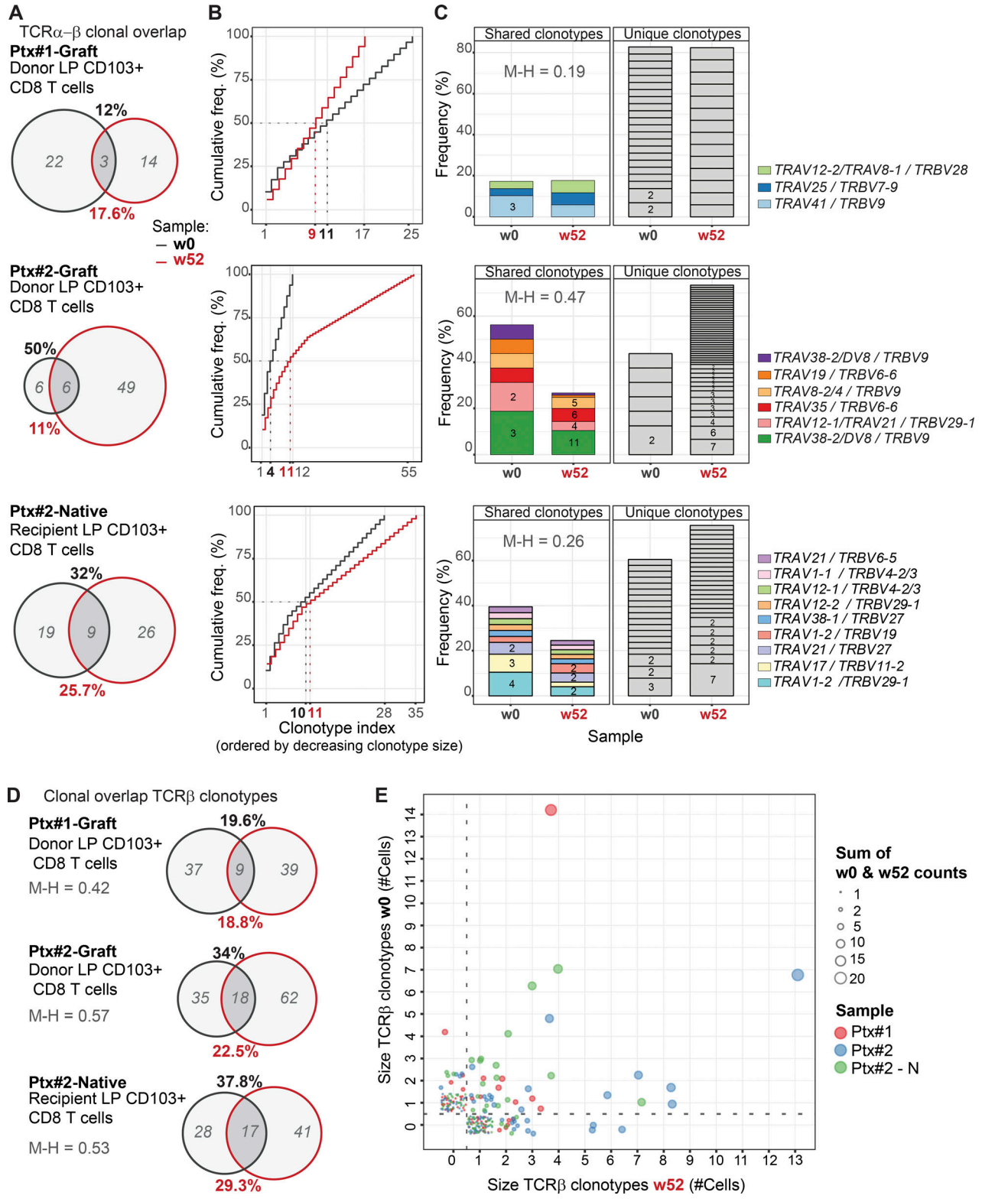

Figure 4. **Persisting clonotypes of CD103⁺ CD8 Trm cells are detected in SI samples 1 yr after Tx. (A)** Clonotype overlap analysis by single-cell TCR-seq of donor CD103⁺ CD8 Trm cells derived from donor duodenum (Ptx#1- and Ptx#2-Donor) at baseline (w0, black) and 52 wk after Tx (w52, red) and of native CD103⁺ CD8 Trms from native duodenum (Ptx#2-Native). In italics (gray), number of unique clonotypes. Clonotype overlap was calculated as follows: % overlap(*X*,*Y*) = [(|*X* ∩ *Y*|)/(|*X*| or |*Y*|)] × 100, where *X* represents the total clonotypes at week 0 (% in black), and *Y* represents the total clonotypes at week 52 (% in red). w, week. **(B)** Frequency (freq.) distribution of LP CD103⁺ CD8 Trm clonotypes at baseline (w0, black line) and 1 yr after Tx (w52, red line). Clonotype index is ordered by decreasing clonotype size. **(C)** Clonal dominance and preferential *TRAV/TRBV* pairing. Each slice of the column represents a different *TRAV/TRBV* pair, and the number of cells expressing them is shown (for more than one cell). Unique and overlapping *TRAV/TRBV* clones are shown separately. **(D)** Clonotype overlap analysis of total TCRβ clonotypes in the same samples as described in A. **(E)** Correlation of the TCRβ clonotypes found at baseline (w0) and 1 yr after Tx (w52). The samples are color-coded, and clonal size is represented by circle size. M-H, Morisita–Horn index.

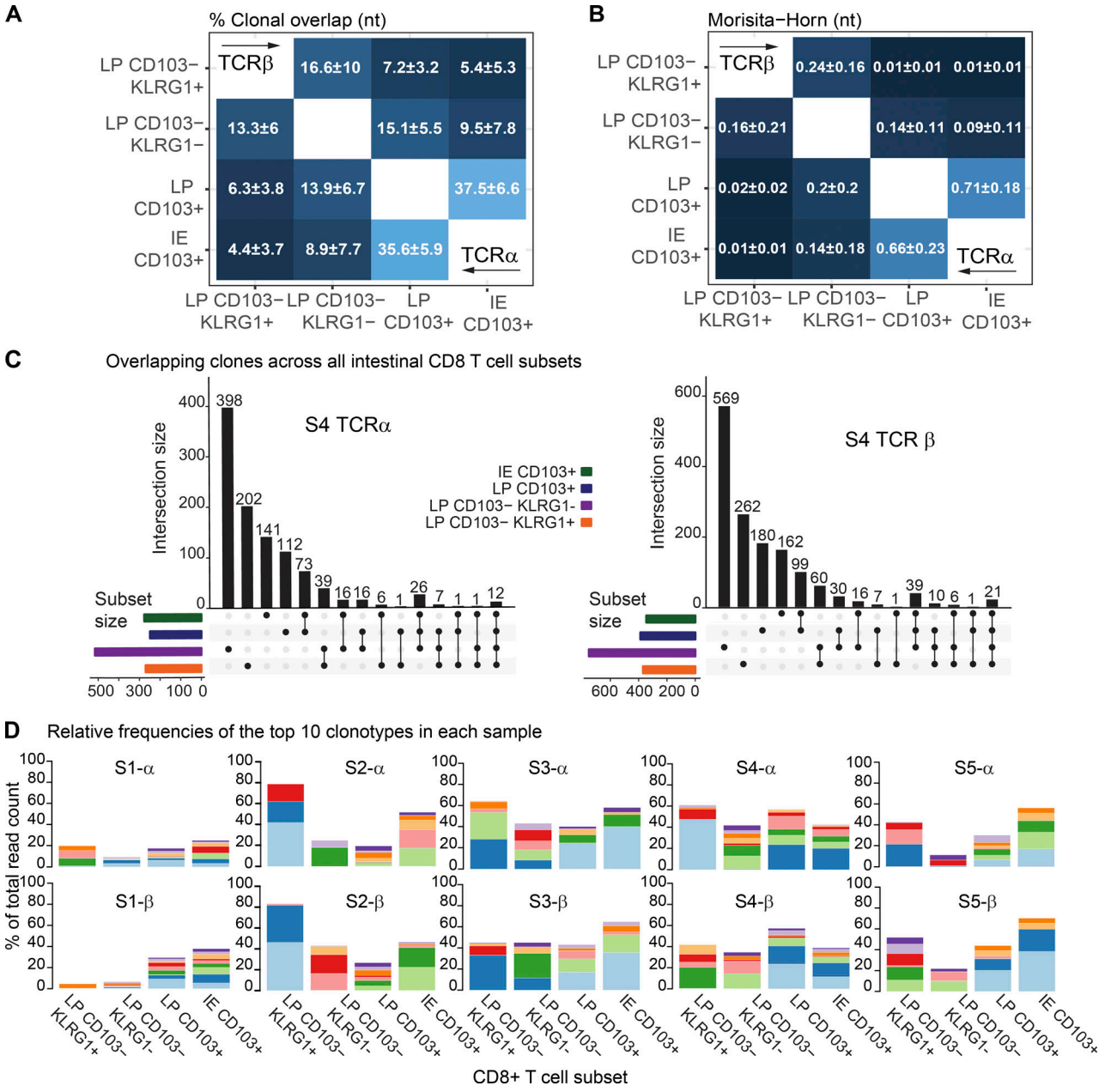

Figure 5. **High clonal overlap between IE and LP CD103⁺ CD8 T cells. (A and B)** Mean percentage of clonal overlap (A) and Morisita–Horn similarity indexes (B) applied to all the pairwise combinations of CD8 T cell subsets for TCRα (right corner) and TCRβ clonotypes (left corner) derived from normal SI (n = 5). The Morisita–Horn index ranges from 0 (no similarity) to 1 (identical). **(C)** Overlapping clones among the different intestinal CD8 T cell subsets for TCRα and TCRβ in one representative sample (n = 5). Intersections are represented below the x axis (black circles), the number of overlapping clonotypes is represented on the histogram, and the total amounts of clonotypes per subset are represented as color-coded horizontal bars. **(D)** Size of the read counts for the 10 most expanded clonotypes relative to the total reads in each subset. Shared clones are represented with the same color within the same sample (S) and TCR chain.

significantly higher levels of the individual cytokines compared with single cytokine–producing cells (Fig. 6, E and F). Within the CD103⁻ CD8 T cell population, we found that KLRG1⁻ cells contained significantly higher numbers of triple-producing cells than their KLRG1⁺ counterpart (Fig. S5 C).

Taken together, these data showed that CD8 Trm cells in LP are more potent cytokine-producing cells than CD103⁻ CD8 T cells. All LP CD8 T cell subsets efficiently produced cytotoxic molecules after activation, whereas IE CD8 Trm cells produced significantly fewer cytokines and cytotoxic molecules.

Discussion

Here we show that the human SI contains several phenotypically, functionally, and clonally distinct CD8 T cell subsets. Virtually all IE CD8 T cells and the majority of LP CD8 T cells expressed a Trm phenotype and were persistent cells (>1 yr) with a very similar immune repertoire. When activated, all subsets contained cytokine-producing cells, with LP CD8 Trm cells being particularly efficient. The two minor CD103⁻ CD8 T cell subsets were phenotypically more similar to PB CD8 T cells, presented an immune repertoire more different from the

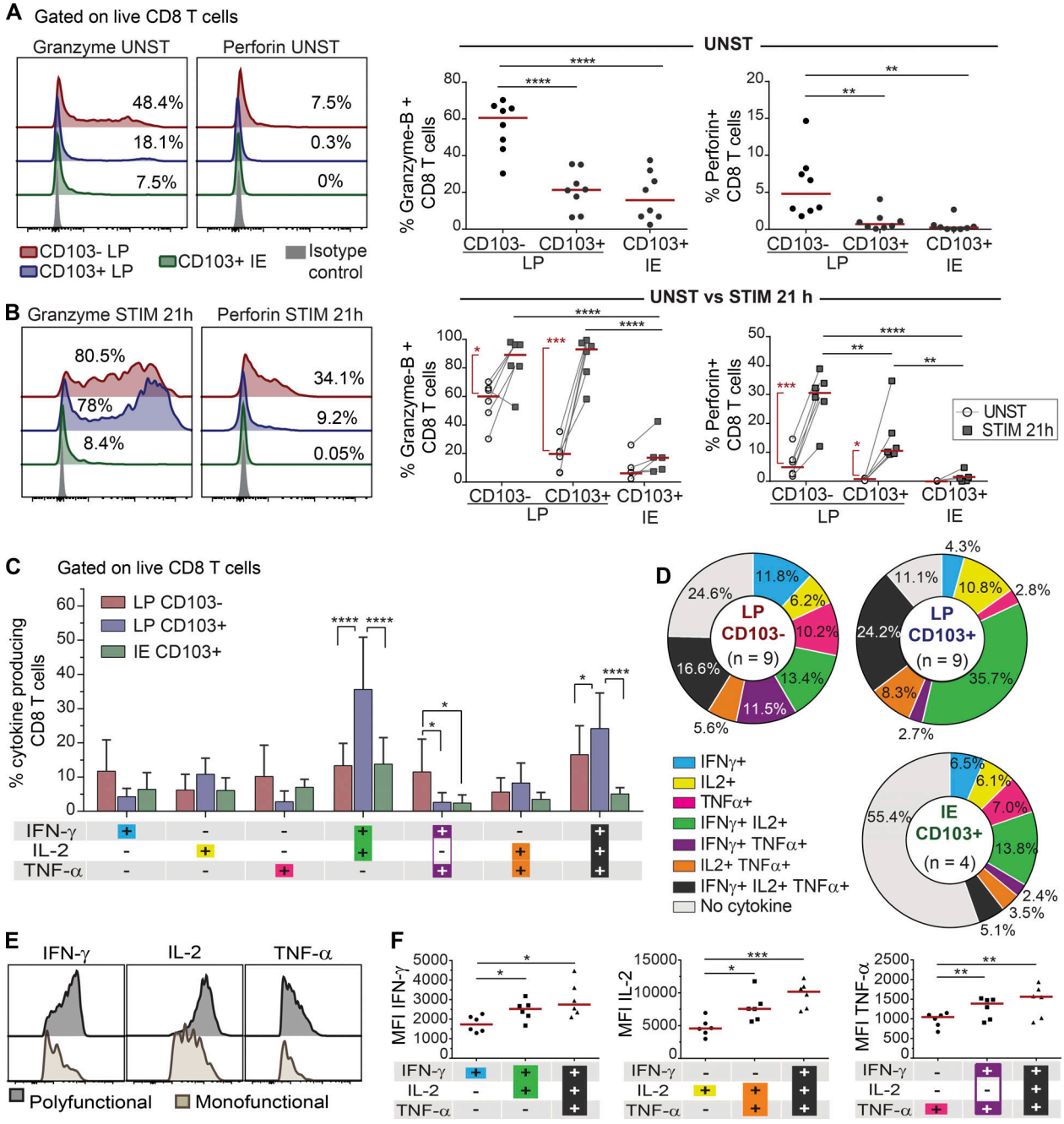

Figure 6. **SI CD8 T cell subsets produce different levels of cytokines and cytotoxic molecules in response to activation. (A and B)** Representative flow-cytometric histogram (left) and compiled data (right, $n = 8$) for the intracellular expression of granzyme-B and perforin in CD8 T cell subsets without (A; UNST) and after (B; STIM) stimulation with anti-CD3/CD28 beads for 21 h ($n = 6$). Red lines indicate median values. **(C)** Flow-cytometric analysis of PMA/ionomycin-induced cytokine production by LP CD103$^-$, LP CD103$^+$, and IE CD103$^+$ CD8 T cells. The mean percentages of cytokine-producing cells with SD are given by bars. **(D)** Relative representation of specific cytokine production profiles for LP CD103$^-$ ($n = 9$), LP CD103$^+$ ($n = 9$), and IE CD103$^+$ ($n = 4$) CD8 T cells are represented on pie charts with color codes (C). Mean values of indicated experiments. **(E and F)** Representative histograms (E) and compiled median fluorescence intensity (MFI; F) values for single, dual, and triple cytokine-producing CD8 T cells ($n = 6$). Red lines indicate median values. Statistical analysis was performed using one-way (A and F) and two-way (B and C) repeated-measures ANOVA with Tukey's multiple comparisons test. For CD3/CD28 stimulation in B, Student's *t* test was applied to compare unstimulated and stimulated cells (red vertical lines and asterisks). *, $P \le 0.05$; **, $P \le 0.01$; ***, $P \le 0.001$; ****, $P \le 0.0001$. Red horizontal lines on graphs represent median values.

Trm cells, and produced higher levels of granzyme-B and perforin.

Experiments to accurately determine the longevity of lymphocytes are not readily performed in human tissues (Landsverk et al., 2017); however, by studying the replacement kinetics in a Tx setting, we were able to determine the persistence of CD8 T cells in grafted human duodenum. By multiparameter flow-cytometric analysis of CD8 T cells derived from normal

(nontransplanted) SI, we found that LP CD8 T cells could be divided into three distinct subsets depending on their expression of CD103 and KLRG1. Most of CD8 T cells displayed a Trm phenotype (CD103$^+$ KLRG1$^-$). We found that LP and IE CD103$^+$ CD8 T cells expressed low levels of CD28, especially in the epithelium. In contrast, LP and IE CD103$^+$ CD8 T cells expressed high levels of natural killer cell receptors, such as 2B4 (SLAM4) and CD161, and high levels of CD127. High PD-1 expression has been reported on CD8 Trm from human lung (Hombrink et al., 2016; Kumar et al., 2017). However, we found that intestinal LP and IE CD103$^+$ express low levels of PD-1, in line with previous studies in mice (Casey et al., 2012). In contrast, the two minor CD103$^-$ subsets in LP, either KLRG1$^-$ or KLRG1$^+$, were more similar to the CD8 T cells in PB, presenting higher levels of CD28, PD1, and NKG2D and lower CD127 and CD161 expression. By following the turnover kinetics of the subsets in transplanted duodenum, we found in half of the patients that >60% of both IE and LP CD103$^+$ CD8 T cells were of donor origin 1 yr after Tx, with no reduction in absolute numbers of CD8 T cells. The finding of persistent donor CD8 T cells was substantiated by single-cell TCR-seq showing a significant clonal overlap between donor LP CD103$^+$ CD8 T cells obtained before and 1 yr after Tx. Donor CD103$^-$ CD8 T cells, in contrast, were more rapidly replaced by recipient cells. However, interestingly, a small fraction (15%) of the CD103$^-$ subsets were still of donor origin 1 yr after Tx.

Zuber et al. (2016) reported that donor CD8 T cells were present in some nonrejected intestinal transplants for >600 d. These patients received intestinal Tx alone or as part of multivisceral Tx, which in both situations included gut-associated lymphoid tissue (GALT, e.g., Peyer's patches) and mesenteric lymph nodes. Long-term mixed chimerism is observed in the blood of these patients (Fu et al., 2019), suggesting that organized lymphatic tissue in the graft continuously expand and release donor T cells that home to the intestinal mucosa. In our study, however, only the proximal part of the duodenum was transplanted, without GALT or lymph nodes, excluding the possibility of continuous replenishment of donor cells after Tx.

Our findings show that CD8 T clones have the capacity to survive for ≥1 yr and most probably many years in the human intestinal mucosa, thus demonstrating the existence of bona fide Trm cells in the human SI. In the steady state, Trm cells can be generated from circulating memory precursors (Gaide et al., 2015) or proliferate locally in response to cognate antigens (Beura et al., 2018a). The proliferation rate, as measured by Ki67 staining, was consistently low in the transplanted and nontransplanted SI. This is in agreement with previous reports (Thome et al., 2014), suggesting that the persistence of CD8 T cells was maintained by long-lived cells rather than local proliferation. The finding that there was no massive expansion of selected clones 1 yr after Tx compared with the situation at baseline and with the native duodenum supports this scenario. Most of the persistent CD8 T cells expressed the classical Trm marker CD103 (αE integrin), which binds E-cadherin on the surface of epithelial cells (Schön et al., 1999). However, a small population of CD103$^-$ CD8 T cells was also maintained for 1 yr in the transplanted duodenum, suggesting that CD103 is not an obligate marker for all Trm cells, as has been also reported for intestinal CD8 T cells in mice (Bergsbaken and Bevan, 2015).

Translated to the steady state situation, it is likely that the turnover rate of CD8 T cells observed in transplanted SI underestimates their physiological longevity for several reasons. First, all patients received immunosuppressive treatment including anti-thymoglobulin, which rapidly depletes T cells in blood (Horneland et al., 2015). It is likely that this treatment also affects the T cell numbers in the periphery. Second, solid organ Tx surgery causes ischemia and reperfusion injury of the graft that increases the turnover of leukocytes (Eguíluz-Gracia et al., 2016); and third, our previous studies have shown that dendritic cells and some of the macrophage subsets are rapidly replaced in the transplanted duodenum (Bujko et al., 2018; Richter et al., 2018), thereby increasing the risk of local alloreactivity. As shown in other Tx settings (lung [Snyder et al., 2019], intestine [Zuber et al., 2016], and kidney [de Leur et al., 2019]), the turnover rate of resident T cells increases with graft rejection. Although patients with histological signs of rejection were excluded from the study, all included patients displayed T cell recipient chimerism in the graft, in which episodes of low-grade rejection cannot be excluded. Altogether, our results, derived from both transplanted and normal SI combined, strongly suggest that virtually all IE CD8 T cells and the majority of LP CD8 T cells under homeostatic conditions are long-lived Trm cells with low proliferative activity (<5% Ki67$^+$ cells).

Most studies of SI CD8 T cells in humans have focused on the IE compartment, and there is less knowledge about the CD8 T cell population in LP. Here we show that IE and LP CD103$^+$ CD8 T cells present a very similar immune repertoire, indicating a common origin. When stimulated with PMA/ionomycin, ∼40% of IE CD8 T cells produced cytokines (IFN-γ, IL-2, or TNF-α), whereas nearly all LP CD8 Trm cells were cytokine producing, and more than a third of these cells produced IFN-γ, IL-2, and TNF-α simultaneously (polyfunctional). This enhanced ability of Trm to produce robust responses mediated by polyfunctional cytokine production have been associated with the role of Trm as sentinel cells in different barrier tissues, such as skin (Watanabe et al., 2015). When activated with anti-CD3/CD28 beads, LP CD8 Trm cells produced high amounts of granzyme-B and significant levels of perforin, whereas IE CD8 T cells expressed less of these cytotoxic mediators. This finding may to some extent be explained by the fact that IE CD8 T cells expressed high levels of immunomodulatory markers (CD244 and CD161, Fig. 2 A) and CD101 (Russell et al., 1996), which may inhibit T cell activation and proliferation. Although IE CD8 T cells were less responsive to the stimuli we used in this study, their TCR repertoire was similar to LP CD103$^+$ CD8 T cells, indicating that they had been activated under similar antigenic conditions. Moreover, in the transplanted intestine, we found that the turnover kinetics of IE and LP CD103$^+$ CD8 T cells were strongly correlated (Fig. S3 C), together suggesting that IE and LP CD8 Trm cells were interrelated populations rather than operating independently in different compartments. Recent reports have shown that murine intestinal T cells are very motile and can move back and forth between the LP and the epithelium (Thompson et al., 2019). In addition, epithelial cells are in

continuous communication with IE CD8 T cells, and it is therefore plausible that epithelial cell signaling under steady state conditions might increase the threshold of TCR-mediated response as a mechanism to maintain the integrity of the epithelial barrier (Jabri and Ebert, 2007).

Approximately 20% of SI CD8 T cells in LP did not express CD103 under steady state conditions. They were phenotypically more similar to PB CD8 T cells than CD8 Trm cells, and the immune repertoire of CD103$^-$ CD8 T cells showed low clonal overlap with their Trm counterparts. In transplanted intestine, incoming recipient CD8 T cells were mainly CD103$^-$ at 3 and 6 wk after Tx, which is compatible with the notion that CD103$^-$ CD8 T cells in the steady state are mostly recently recruited cells. However, 1 yr after Tx, most recipient CD8 T cells presented a Trm phenotype, indicating that CD103$^-$ CD8 T cells differentiated into CD8 Trm cells in situ. Comparing the TCR repertoire, CD103$^-$ KLRG1$^-$ CD8 T cells were more similar to CD8 Trm cells than CD103$^-$ KLRG1$^+$ cells, which agrees with studies in mice showing that KLRG1$^-$ CD8 T cells are Trm precursors (Mackay et al., 2013; Sheridan et al., 2014). The KLRG1$^-$ subset was also more similar to Trm cells with regard to production of cytokines and cytotoxic molecules. Notwithstanding these findings, it has been shown that TGF-β, abundantly present in the intestinal microenvironment, induces down-regulation of KLRG1 (Schwartzkopff et al., 2015). Thus, it is possible that also KLRG1$^+$ T cells can differentiate into Trm cells (Herndler-Brandstetter et al., 2018).

Interestingly, the immune repertoire in both CD103$^+$ and CD103$^-$ subsets was polarized toward few dominating expanded clones. Assuming that CD103$^-$ CD8 T cells were recently recruited from the circulation, this finding suggests that the clonal expansion had occurred before disseminating into the tissue, most likely in GALT and mesenteric lymph nodes. In agreement with this concept, biopsies obtained from different sites (several centimeters apart) and at different time points in transplanted patients showed expansion of many of the same clones, suggesting that T cell clones were evenly distributed along the duodenal mucosa and less dependent on local proliferation. Thus, the maintenance of a polarized immune repertoire (likely specific to recurrent pathogens), conserved both longitudinally in the tissue and over time, represents an optimized strategy of protection.

There is increasing evidence that Trm cells play an important role in mediating protective responses and maintaining long-term immunity against a broad variety of infectious diseases (Muruganandah et al., 2018). These studies are mainly performed in mouse models, and studies investigating the existence and function of Trm cells in human tissue are still few. Here we provide evidence that the majority of SI CD8 T cells in the steady state are long-lived cells with very highly potent protective capabilities. These data indicate that Trm cells in the intestinal mucosa are attractive targets to design effective oral vaccines. Further, the knowledge that long-lived T cells exist in the gut should give incentive for the implementation of new therapeutic strategies in diseases where pathogenic T cells play an important role, such as inflammatory bowel disease, celiac disease, and gut graft-versus-host disease.

Materials and methods

Human biological material

SI samples were obtained either during pancreatic cancer surgery (Whipple procedure, n = 35; mean age 63 yr, range 40–81; 16 female) or from donors or patients during pancreas-duodenum Tx (donors, n = 52; mean age 31 yr, range 5–55; 24 female; patients, n = 36; mean age 41 yr, range 25–60; 14 female) as described previously (Landsverk et al., 2017; Richter et al., 2018). Cancer patients receiving neoadjuvant chemotherapy were excluded from the study. Endoscopic biopsies from donor and patient duodenum were obtained 3, 6, and 52 wk after Tx. All transplanted patients received a standard immunosuppressive regimen (Horneland et al., 2015). All tissue specimens were evaluated blindly by experienced pathologists, and only material with normal histology was included (Ruiz et al., 2010). Transplanted patients showing clinical or histological signs of rejection or other complications, as well as patients presenting pretransplant or de novo donor-specific antibodies, were excluded from the study. Blood samples were collected at the time of surgery, and buffy coats from healthy donors (Oslo University Hospital, Oslo, Norway).

Intestinal resections were opened longitudinally and rinsed with PBS, and mucosa was dissected in strips off the submucosa. For microscopy, small mucosal pieces were fixed in 4% formalin and embedded in paraffin according to standard protocols. Intestinal mucosa was washed three times in PBS containing 2 mM EDTA and 1% FCS at 37°C with shaking for 20 min and filtered through nylon 100-µm mesh to remove epithelial cells. Epithelial fractions in each washing step were pooled and filtered through 100-µm cell strainers (Falcon; BD). After three sequential washes with EDTA buffer, the epithelial layer was completely removed from the tissue, and the basal membrane remained intact as shown in Fig. S1 A. Epithelial cells in the EDTA fraction were depleted by incubation with anti-human epithelial antigen antibody (clone Ber-EP4; Dako) followed by anti-mouse IgG Dynabeads (Thermo Fisher Scientific) according to the manufacturer's protocol. A death cell removal kit (Miltenyi) was applied to the depleted IE cells before cell sorting and functional assays. LP was minced and digested in complete RPMI medium (supplemented with 10% FCS and 1% penicillin/streptomycin) containing 0.25 mg/ml Liberase TL and 20 U/ml DNase I (both from Roche), with stirring at 37°C for 1 h. Digested tissue was filtered twice through 100-µm cell strainers and washed three times in PBS. The purity of both IE and LP fractions was checked by flow cytometry. We found <5% BerEP4$^+$ epithelial cells in LP and no expression of B cell/plasma cell markers (CD19 or CD27) in the IE (Fig. S1 B), confirming that the degree of cross-contamination between these fractions was very low. Intestinal biopsies from transplanted patients were processed according to the same protocol. PBMCs were isolated by Ficoll-based density gradient centrifugation (Lymphoprep; Axis-Shield). All participants gave their written informed consent. The study was approved by the Regional Committee for Medical Research Ethics in Southeast Norway and complies with the Declaration of Helsinki.

Microscopy

Analysis of chimerism was performed as described previously (Landsverk et al., 2017). Briefly, formalin-fixed 4-µm sections

were washed sequentially in xylene, ethanol, and PBS. Heat-induced epitope retrieval was performed by boiling sections for 20 min in Dako buffer. Sections were incubated with CEP X SpectrumOrange/Y SpectrumGreen DNA Probes (Abbott Molecular) for 12 h at 37°C before immunostaining according to standard protocol with anti-CD3 (Polyclonal; Dako), anti-CD8 (clone 4B11; Novocastra) and secondary antibodies targeting rabbit IgG or mouse IgG2b conjugated to Alexa Fluor 647 and 555, respectively. Laser scanning confocal microscopy was performed on an Olympus FV1000 (BX61WI) system. Image z stacks were acquired at 1-µm intervals and combined using the Z project maximum-intensity function in ImageJ (National Institutes of Health). All microscopy images were assembled in Photoshop and Illustrator CC (Adobe).

CD8 immunoenzymatic staining was performed on formalin-fixed 4-µm sections, dewaxed in xylene and rehydrated in ethanol, and prepared with Vulcan Fast red kit (Biocare Medical) following standard protocols. In brief, heat-induced antigen retrieval was performed in Tris/EDTA pH 9 buffer, followed by staining with primary antibody (CD8 clone 4B11; Novocastra) and secondary anti-mouse AP-conjugated antibody and incubation with substrate (Fast Red Chromogen; Biocare Medical). Slides were counterstained with hematoxylin, and excess dye was removed by bluing in ammonia water. Tissue sections were scanned using Pannoramic Midi slide scanner (3DHISTECH), and counts were generated with QuPath software (Bankhead et al., 2017).

Flow cytometry and cell sorting

Immunophenotyping was performed on single-cell suspensions of LP and IE fractions and PBMCs using different multicolor combinations of directly conjugated monoclonal antibodies (Table S1). To assess the expression of L-selectin on digested tissue, cells were rested for 12 h at 37°C before immunostaining. Replacement of donor cells in duodenal biopsies of HLA-mismatched transplanted patients was assessed using different HLA type I allotype-specific antibodies targeting donor- and/or recipient-derived cells, and stroma cells were used as a control of specific staining. Dead cells were excluded based on propidium iodide staining (Molecular Probes; Life Technologies).

For analysis of cytokine production, LP and IE cell suspensions were stimulated for 4 h with control complete medium (RPMI supplemented with 10% FCS and 1% penicillin/streptomycin) or PMA (1.5 ng/ml) and ionomycin (1 µg/ml; both from Sigma-Aldrich) in the presence of monensin (Golgi Stop; BD Biosciences) added after 1 h of stimulation to allow intracellular accumulation of cytokines. Cells were stained using the BD Cytofix/Cytoperm kit (BD Biosciences) according to the manufacturer's instructions and stained with antibodies against TNFα, IFNγ, or IL-2 (Table S1). The mean percentage of live cells in the cytokine experiments, determined by flow-cytometric analysis using a fixable viability dye, was 77% for LP CD8 T cells (range 58.8–92.8%) and 70% for IE CD8 T cells (range 56.9–83.4%). For detection of cytotoxic granules, LP and IE cells were activated for 21 h with anti-CD3/CD28 beads (Dynabeads; Thermo Fisher Scientific) or control complete medium. For detection of intranuclear Ki67 expression, the FoxP3/transcription factor staining buffer set was used according to the manufacturer's instructions. eFluor-450 or eFluor-780 fixable viability dyes (eBioscience) were used before any intracellular/intranuclear staining procedure. All samples were acquired on LSR Fortessa flow cytometer (BD Biosciences), using FACSDiva software (BD Biosciences). Single-stained controls were prepared for compensation (UltraComp eBeads; eBioscience), and gates were adjusted by comparison with FMO controls or matched isotype controls.

Flow cytometry data were analyzed using FlowJo 10.4.2 (TreeStar). For Fig. 1 C, the expression of 16 phenotypic markers was analyzed at the single-cell level and compared for CD8 T cells in PB, LP, and IE (n = 5) using the merge and calculation functions of Infinicyt software (Cytognos), as described in detail elsewhere (Pedreira et al., 2013). The population within the CD8 T cell gate was downsampled for each compartment and exported to a new file, and then concatenated and subjected to t-SNE analysis using the plugin integrated in FlowJo 10.4.2 (see Fig. S2 A for more details). FACS sorting was performed on an Aria II Cell Sorter (BD Biosciences). A TCRγδ antibody was used to exclude these cells during sorting (see gating strategy in Fig. S4 A). All experiments were performed at the Flow Cytometry Core Facility, Oslo University Hospital.

Single-cell TCRα-β sequencing

Cell suspensions from two donors (Ptx#1 and Ptx#2) were prepared at the time of Tx and kept frozen in liquid nitrogen. 1 yr after Tx, biopsies from the same patients (donor and recipient tissue) were collected, and single-cell suspensions were prepared and processed together with the thawed baseline samples from the same patients. Donor $CD103^+$ $KLRG1^-$ CD8 T cells from LP of transplanted tissue were identified following the gating strategy in Fig. S4 A, and single cells were sorted into 96-well plates (Bio-Rad) containing 5 µl capture buffer (20 mM Tris-HCl, pH 8, 1% NP-40, and 1 U/µl RNase inhibitor). The plates were spun down and snap frozen immediately after sorting and stored at −80°C until cDNA synthesis. Paired TCRα and TCRβ sequences were obtained after three nested PCRs with multiplexed primers covering all TCRα and TCRβ V genes, as described before (Risnes et al., 2018). In brief, cDNA plates were stored at −20°C, and each of the three nested PCR steps was performed in a total volume of 10 µl using 1 µl cDNA/PCR template and KAPA HiFi HotStart ReadyMix (Kapa Biosystems). In the last PCR reaction, *TRAC* and *TRBC* barcoding primers were added together with Illumina PairedEnd primers. Cycling conditions, concentrations, and primer sequences for all three PCR reactions can be found in Risnes et al. (2018) and the original protocol in Han et al. (2014). Products in each well were combined, purified, and sequenced using the Illumina paired-end 250-bp MiSeq platform at the Norwegian Sequencing Centre, Oslo University Hospital. The resulting paired-end sequencing reads were processed in a multistep pipeline using selected steps of the pRESTO toolkit (Vander Heiden et al., 2014) according to Risnes et al. (2018). In short, high-purity reads (average Phred score >30) were deconvoluted using barcode identifiers and collapsed, and only the top three for each well were retained for further analysis. For identification of V, D, and J genes and the CDR3

junctions, the International ImMunoGeneTics Information System (IMGT)/HighV-QUEST online tool (Alamyar et al., 2012) was used. The results were then filtered and collapsed. Paired TCR sequences were grouped in clonotypes, defined by identical V and J gene (subgroup level) together with identical CDR3 nucleotide sequence for both TCRα and TCRβ when that information was available (Brown et al., 2019). Only valid singleton cells containing no more than three chains (dual TCRα and TCRβ) with ≥100 reads were considered for downstream analysis.

Bulk TCR-seq

5,000 cells of each subset of CD8 T cells (CD103$^-$ KLRG1$^+$, CD103$^-$ KLRG1$^-$, and CD103$^+$ from LP and CD103$^+$ IELs) were sorted into tubes containing 100 µl of TCL lysis buffer (Qiagen) supplemented with 1% β-mercaptoethanol and stored at −80°C until cDNA synthesis (see Fig. S4 B). Total RNA was extracted using RNAclean XP beads (Agencourt) following the manufacturer's protocol. A modified SMART (switching mechanism at 5′ end of RNA template) protocol (Quigley et al., 2011) was used in first-strand cDNA synthesis, described in detail elsewhere (Risnes et al., 2018). In brief, TCRα and TCRβ genes were amplified in two rounds of seminested PCRs. In the first reaction, the cDNA from each sample was divided into three replicates and amplified with *TRAC* and *TRBC* primers, and in the second reaction, different indexed primers were used to barcode the samples and replicates. A third, final reaction was performed using Illumina Seq Primers R1/R2 for sequencing. TCRα and TCRβ PCR products were quantified using the KAPA library quantification kit for Illumina platforms (Kapa Biosystems) and pooled at the same concentrations. Subsequently, pooled TCRα and TCRβ products were cleaned and concentrated with MinElute PCR Purification Kit (Qiagen) and run on a 1.5% agarose gel. Bands of appropriate size (~650 bp) were gel-extracted (Fig. S4 C), purified using the Monarch Gel Extraction kit (New England Biolabs), and cleaned with MinElute PCR Purification Kit. The amplicon TCR library was sequenced using the paired-end 300-bp Illumina MiSeq; the approximate number of paired-end reads generated per CD8 T cell population was 35,000 reads for TCRα and 45,000 reads for TCRβ sequences. The total number of reads was 60 million (~20 million reads per library). Bulk TCR-seq data were preprocessed (VDJ alignment and clonotyping) using the MiXCR software package (Bolotin et al., 2015). Clonotypes were defined based on the V and J gene usage and the nucleotide sequence of the CDR3 region (Greiff et al., 2015b). Correlation of the read counts for the clonotypes found within the three molecular replicates was high (Fig. S4 D), indicating reproducibility of the TCR repertoire sequencing (Greiff et al., 2014). For downstream analysis, raw reads from molecular triplicates were cumulated, and only clonotypes with a minimal read count of 10 were used. Sample preparation and read statistics are summarized in Fig. S4 (B–E). tcR package was used for descriptive statistics (Nazarov et al., 2015). The percentage of overlapping clones shared between two CD8 T cell subsets was calculated as

$$\text{overlap}(X, Y) = \frac{|X \cap Y|}{\text{mean}(|X|, |Y|)} \times 100,$$

where $|X|$ and $|Y|$ are the clonal sizes (number of unique clones) of repertoires X and Y.

Statistical analysis

Statistical analyses were performed in Prism 7 (GraphPad Software). To assess statistical significance among SI CD8 T cell subsets, data were analyzed by one-way ANOVA (standard or repeated measures) followed by Tukey's multiple comparison tests. Replacement data and distribution of CD8 T cell subsets at different time points were analyzed by two-way ANOVA matching across subsets, followed by Tukey's multiple comparison tests. Correlations between replacement kinetics of different CD8 T cell subsets were calculated using Pearson correlation with two-tailed P value (95% confidence interval). P values of <0.05 were considered significant. TCR repertoire analysis was performed using the R statistical programming environment (R Development Core Team, 2018). Non-base R packages used for analyses were tcR (Nazarov et al., 2015), upsetR (Lex et al., 2014), ggplot2 (Wickham, 2009), and VennDiagram (Chen, 2018). The Morisita–Horn index was calculated using the R divo package (Sadee et al., 2017). Vegan package (Oksanen et al., 2018) was used to calculate the diversity (Shannon evenness index) as previously described (Greiff et al., 2015a).

Data and materials availability

Bulk and single-cell TCR raw sequences were deposited under a controlled data access at the European Genome-phenome Archive (https://www.ebi.ac.uk/ega/), with the accession no. EGAS00001003676 (datasets EGAD00001005049 and EGAD00001005050, respectively).

Online supplemental material

Fig. S1 shows some general considerations regarding sample preparation and characterization of intestinal CD8 T cells. Fig. S2 depicts extended features of the immunophenotypic analysis applied to PB, LP, and IE CD8 T cells. Fig. S3 summarizes additional data concerning the replacement kinetics of intestinal CD8 T cells in transplanted duodenum. Fig. S4 provides information about the TCR immune repertoire analysis: Gating strategy for sorting, bulk TCR-seq workflow, and read statistics. Fig. S5 shows functional characterization of LP KLRG1$^+$ and KLRG1$^-$ CD103$^-$ CD8 T cell subsets. Table S1 lists all the antibodies used in the study.

Acknowledgments

We are grateful to Kjersti Thorvaldsen Hagen, Frank Sætre, and Kathrine Hagelsteen for excellent technical assistance; the staff at the Endoscopy Unit and the surgery theater; Christian Naper for providing HLA typing; the Confocal Microscopy and Flow Cytometry Core Facilities at Oslo University Hospital, Rikshospitalet; and Thomas S. Kupper (Department of Dermatology, Harvard Medical School, Cambridge, MA) for critical reading of the manuscript.

This work was partly supported by the Research Council of Norway through its Centres of Excellence funding scheme

(project number 179573/V40) and by grant from the South Eastern Norway Regional Health Authority (project number 2015002).

The authors declare no competing financial interests.

Author contributions: R. Bartolomé-Casado, O.J.B. Landsverk, E.S. Bækkevold, and F.L. Jahnsen conceived the project. R. Bartolomé-Casado, O.J.B. Landsverk, and S.K. Chauhan processed samples, designed and performed experiments, and analyzed data. L. Richter helped establish methodology and advised on advanced flow-cytometry analysis. D. Phung and L.F. Risnes assisted in experiments. V. Greiff provided critical insights and assisted in bioinformatic analysis and design of figures. R.S. Neumann, Y. Yao, and V. Greiff developed bioinformatic tools. S. Yaqub and R. Horneland coordinated recruitment of patients and collection of biopsies. S. Yaqub, R. Horneland, O. Øyen, and E.M. Aandahl performed surgery and provided biopsies. V. Paulsen performed endoscopy and provided endoscopic biopsies. R. Bartolomé-Casado performed bioinformatic analysis and prepared figures. R. Bartolomé-Casado and F.L. Jahnsen wrote the manuscript. O.J.B. Landsverk, S.K. Chauhan, V. Greiff, L. Richter, D. Phung, L.F. Risnes, E.M. Aandahl, S-W. Qiao, L.M. Sollid, and E.S. Baekkevold contributed to writing the manuscript. S-W. Qiao, E.S. Baekkevold, and F.L. Jahnsen supervised the study.

Submitted: 6 March 2019
Revised: 13 May 2019
Accepted: 20 June 2019

References

Abadie, V., V. Discepolo, and B. Jabri. 2012. Intraepithelial lymphocytes in celiac disease immunopathology. *Semin. Immunopathol.* 34:551–566. https://doi.org/10.1007/s00281-012-0316-x

Alamyar, E., P. Duroux, M.P. Lefranc, and V. Giudicelli. 2012. IMGT(®) tools for the nucleotide analysis of immunoglobulin (IG) and T cell receptor (TR) V-(D)-J repertoires, polymorphisms, and IG mutations: IMGT/V-QUEST and IMGT/HighV-QUEST for NGS. *Methods Mol. Biol.* 882: 569–604. https://doi.org/10.1007/978-1-61779-842-9_32

Ariotti, S., M.A. Hogenbirk, F.E. Dijkgraaf, L.L. Visser, M.E. Hoekstra, J.Y. Song, H. Jacobs, J.B. Haanen, and T.N. Schumacher. 2014. T cell memory. Skin-resident memory CD8+ T cells trigger a state of tissue-wide pathogen alert. *Science.* 346:101–105. https://doi.org/10.1126/science.1254803

Bankhead, P., M.B. Loughrey, J.A. Fernández, Y. Dombrowski, D.G. McArt, P.D. Dunne, S. McQuaid, R.T. Gray, L.J. Murray, H.G. Coleman, et al. 2017. QuPath: Open source software for digital pathology image analysis. *Sci. Rep.* 7:16878. https://doi.org/10.1038/s41598-017-17204-5

Bergsbaken, T., and M.J. Bevan. 2015. Proinflammatory microenvironments within the intestine regulate the differentiation of tissue-resident CD8+ T cells responding to infection. *Nat. Immunol.* 16:406–414. https://doi.org/10.1038/ni.3108

Beura, L.K., J.S. Mitchell, E.A. Thompson, J.M. Schenkel, J. Mohammed, S. Wijeyesinghe, R. Fonseca, B.J. Burbach, H.D. Hickman, V. Vezys, et al. 2018a. Intravital mucosal imaging of CD8+ resident memory T cells shows tissue-autonomous recall responses that amplify secondary memory. *Nat. Immunol.* 19:173–182. https://doi.org/10.1038/s41590-017-0029-3

Beura, L.K., S. Wijeyesinghe, E.A. Thompson, M.G. Macchietto, P.C. Rosato, M.J. Pierson, J.M. Schenkel, J.S. Mitchell, V. Vezys, B.T. Fife, et al. 2018b. T Cells in Nonlymphoid Tissues Give Rise to Lymph-Node-Resident Memory T Cells. *Immunity.* 48:327–338.e5. https://doi.org/10.1016/j.immuni.2018.01.015

Bolotin, D.A., S. Poslavsky, I. Mitrophanov, M. Shugay, I.Z. Mamedov, E.V. Putintseva, and D.M. Chudakov. 2015. MiXCR: software for comprehensive adaptive immunity profiling. *Nat. Methods.* 12: 380–381. https://doi.org/10.1038/nmeth.3364

Brown, A.J., I. Snapkov, R. Akbar, M. Pavlović, E. Miho, G.K. Sandve, and V. Greiff. 2019. Augmenting adaptive immunity: progress and challenges in the quantitative engineering and analysis of adaptive immune receptor repertoires. *arXiv.* doi:arXiv:1904.04105v2 [q-bio.QM] (Preprint posted April 8, 2019)

Bujko, A., N. Atlasy, O.J.B. Landsverk, L. Richter, S. Yaqub, R. Horneland, O. Øyen, E.M. Aandahl, L. Aabakken, H.G. Stunnenberg, et al. 2018. Transcriptional and functional profiling defines human small intestinal macrophage subsets. *J. Exp. Med.* 215:441–458. https://doi.org/10.1084/jem.20170057

Casey, K.A., K.A. Fraser, J.M. Schenkel, A. Moran, M.C. Abt, L.K. Beura, P.J. Lucas, D. Artis, E.J. Wherry, K. Hogquist, et al. 2012. Antigen-independent differentiation and maintenance of effector-like resident memory T cells in tissues. *J. Immunol.* 188:4866–4875. https://doi.org/10.4049/jimmunol.1200402

Chen, H.2018. VennDiagram: Generate High-Resolution Venn and Euler Plots. Available at: https://rdrr.io/cran/VennDiagram/ (accessed July 17, 2018).

de Leur, K., M. Dieterich, D.A. Hesselink, O.B.J. Corneth, F.J.M.F. Dor, G.N. de Graav, A.M.A. Peeters, A. Mulder, H.J.A.N. Kimenai, F.H.J. Claas, et al. 2019. Characterization of donor and recipient CD8+ tissue-resident memory T cells in transplant nephrectomies. *Sci. Rep.* 9:5984. https://doi.org/10.1038/s41598-019-42401-9

Eguíluz-Gracia, I., H.H. Schultz, L.I. Sikkeland, E. Danilova, A.M. Holm, C.J. Pronk, W.W. Agace, M. Iversen, C. Andersen, F.L. Jahnsen, and E.S. Baekkevold. 2016. Long-term persistence of human donor alveolar macrophages in lung transplant recipients. *Thorax.* 71:1006–1011. https://doi.org/10.1136/thoraxjnl-2016-208292

Fergusson, J.R., M.H. Hühn, L. Swadling, L.J. Walker, A. Kurioka, A. Llibre, A. Bertoletti, G. Holländer, E.W. Newell, M.M. Davis, et al. 2016. CD161(int) CD8+ T cells: a novel population of highly functional, memory CD8+ T cells enriched within the gut. *Mucosal Immunol.* 9:401–413. https://doi.org/10.1038/mi.2015.69

Fu, J., J. Zuber, M. Martinez, B. Shonts, A. Obradovic, H. Wang, S.P. Lau, A. Xia, E.E. Waffarn, K. Frangaj, et al. 2019. Human intestinal allografts contain functional hematopoietic stem and progenitor cells that are maintained by a circulating pool. *Cell Stem Cell.* 24:227–239.e8. https://doi.org/10.1016/j.stem.2018.11.007

Gaide, O., R.O. Emerson, X. Jiang, N. Gulati, S. Nizza, C. Desmarais, H. Robins, J.G. Krueger, R.A. Clark, and T.S. Kupper. 2015. Common clonal origin of central and resident memory T cells following skin immunization. *Nat. Med.* 21:647–653. https://doi.org/10.1038/nm.3860

Gola, A., D. Silman, A.A. Walters, S. Sridhar, S. Uderhardt, A.M. Salman, B.R. Halbroth, D. Bellamy, G. Bowyer, J. Powlson, et al. 2018. Prime and target immunization protects against liver-stage malaria in mice. *Sci. Transl. Med.* 10:eaap9128. https://doi.org/10.1126/scitranslmed.aap9128

Greiff, V., U. Menzel, U. Haessler, S.C. Cook, S. Friedensohn, T.A. Khan, M. Pogson, I. Hellmann, and S.T. Reddy. 2014. Quantitative assessment of the robustness of next-generation sequencing of antibody variable gene repertoires from immunized mice. *BMC Immunol.* 15:40. https://doi.org/10.1186/s12865-014-0040-5

Greiff, V., P. Bhat, S.C. Cook, U. Menzel, W. Kang, and S.T. Reddy. 2015a. A bioinformatic framework for immune repertoire diversity profiling enables detection of immunological status. *Genome Med.* 7:49. https://doi.org/10.1186/s13073-015-0169-8

Greiff, V., E. Miho, U. Menzel, and S.T. Reddy. 2015b. Bioinformatic and Statistical Analysis of Adaptive Immune Repertoires. *Trends Immunol.* 36:738–749. https://doi.org/10.1016/j.it.2015.09.006

Han, A., J. Glanville, L. Hansmann, and M.M. Davis. 2014. Linking T-cell receptor sequence to functional phenotype at the single-cell level. *Nat. Biotechnol.* 32:684–692. https://doi.org/10.1038/nbt.2938

Herndler-Brandstetter, D., H. Ishigame, R. Shinnakasu, V. Plajer, C. Stecher, J. Zhao, M. Lietzenmayer, L. Kroehling, A. Takumi, K. Kometani, et al. 2018. KLRG1+ Effector CD8+ T Cells Lose KLRG1, Differentiate into All Memory T Cell Lineages, and Convey Enhanced Protective Immunity. *Immunity.* 48:716–729.e8. https://doi.org/10.1016/j.immuni.2018.03.015

Hombrink, P., C. Helbig, R.A. Backer, B. Piet, A.E. Oja, R. Stark, G. Brasser, A. Jongejan, R.E. Jonkers, B. Nota, et al. 2016. Programs for the persistence, vigilance and control of human CD8+ lung-resident memory T cells. *Nat. Immunol.* 17:1467–1478. https://doi.org/10.1038/ni.3589

Horneland, R., V. Paulsen, J.P. Lindahl, K. Grzyb, T.J. Eide, K. Lundin, L. Aabakken, T. Jenssen, E.M. Aandahl, A. Foss, and O. Øyen. 2015. Pancreas transplantation with enteroanastomosis to native duodenum

poses technical challenges--but offers improved endoscopic access for scheduled biopsies and therapeutic interventions. *Am. J. Transplant.* 15: 242–250. https://doi.org/10.1111/ajt.12953

Jabri, B., and E. Ebert. 2007. Human CD8+ intraepithelial lymphocytes: a unique model to study the regulation of effector cytotoxic T lymphocytes in tissue. *Immunol. Rev.* 215:202–214. https://doi.org/10.1111/j.1600-065X.2006.00481.x

Konjar, Š., U.C. Frising, C. Ferreira, R. Hinterleitner, T. Mayassi, Q. Zhang, B. Blankenhaus, N. Haberman, Y. Loo, J. Guedes, et al. 2018. Mitochondria maintain controlled activation state of epithelial-resident T lymphocytes. *Sci. Immunol.* 3:eaan2543. https://doi.org/10.1126/sciimmunol.aan2543

Kumar, B.V., W. Ma, M. Miron, T. Granot, R.S. Guyer, D.J. Carpenter, T. Senda, X. Sun, S.H. Ho, H. Lerner, et al. 2017. Human Tissue-Resident Memory T Cells Are Defined by Core Transcriptional and Functional Signatures in Lymphoid and Mucosal Sites. *Cell Reports.* 20:2921–2934. https://doi.org/10.1016/j.celrep.2017.08.078

Landsverk, O.J., O. Snir, R.B. Casado, L. Richter, J.E. Mold, P. Réu, R. Horneland, V. Paulsen, S. Yaqub, E.M. Aandahl, et al. 2017. Antibody-secreting plasma cells persist for decades in human intestine. *J. Exp. Med.* 214:309–317. https://doi.org/10.1084/jem.20161590

Lex, A., N. Gehlenborg, H. Strobelt, R. Vuillemot, and H. Pfister. 2014. UpSet: Visualization of Intersecting Sets. *IEEE Trans. Vis. Comput. Graph.* 20: 1983–1992. https://doi.org/10.1109/TVCG.2014.2346248

Mackay, L.K., A. Rahimpour, J.Z. Ma, N. Collins, A.T. Stock, M.L. Hafon, J. Vega-Ramos, P. Lauzurica, S.N. Mueller, T. Stefanovic, et al. 2013. The developmental pathway for CD103(+)CD8+ tissue-resident memory T cells of skin. *Nat. Immunol.* 14:1294–1301. https://doi.org/10.1038/ni.2744

Maynard, C.L., C.O. Elson, R.D. Hatton, and C.T. Weaver. 2012. Reciprocal interactions of the intestinal microbiota and immune system. *Nature.* 489:231–241. https://doi.org/10.1038/nature11551

McDonald, B.D., B. Jabri, and A. Bendelac. 2018. Diverse developmental pathways of intestinal intraepithelial lymphocytes. *Nat. Rev. Immunol.* 18:514–525. https://doi.org/10.1038/s41577-018-0013-7

Muruganandah, V., H.D. Sathkumara, S. Navarro, and A. Kupz. 2018. A Systematic Review: The Role of Resident Memory T Cells in Infectious Diseases and Their Relevance for Vaccine Development. *Front. Immunol.* 9:1574. https://doi.org/10.3389/fimmu.2018.01574

Nazarov, V.I., M.V. Pogorelyy, E.A. Komech, I.V. Zvyagin, D.A. Bolotin, M. Shugay, D.M. Chudakov, Y.B. Lebedev, and I.Z. Mamedov. 2015. tcR: an R package for T cell receptor repertoire advanced data analysis. *BMC Bioinformatics.* 16:175. https://doi.org/10.1186/s12859-015-0613-1

Oksanen, J., F.G. Blanchet, M. Friendly, R. Kindt, P. Legendre, D. McGlinn, P.R. Minchin, R.B. O'Hara, G.L. Simpson, P. Solymos, et al. 2018. vegan: Community Ecology Package. Available at: https://cran.r-project.org/package=vegan (accessed July 17, 2018).

Park, S.L., A. Buzzai, J. Rautela, J.L. Hor, K. Hochheiser, M. Effern, N. McBain, T. Wagner, J. Edwards, R. McConville, et al. 2019. Tissue-resident memory CD8$^+$ T cells promote melanoma-immune equilibrium in skin. *Nature.* 565:366–371. https://doi.org/10.1038/s41586-018-0812-9

Pedreira, C.E., E.S. Costa, Q. Lecrevisse, J.J. van Dongen, and A. Orfao. EuroFlow Consortium. 2013. Overview of clinical flow cytometry data analysis: recent advances and future challenges. *Trends Biotechnol.* 31: 415–425. https://doi.org/10.1016/j.tibtech.2013.04.008

Quigley, M.F., J.R. Almeida, D.A. Price, and D.C. Douek. 2011. Unbiased molecular analysis of T cell receptor expression using template-switch anchored RT-PCR. *Curr. Protoc. Immunol.* Chapter 10:Unit 10.33.

R Development Core Team. 2018. R: A Language and Environment for Statistical Computing. R Foundation for Statistical Computing, Vienna, Austria.

Richter, L., O.J.B. Landsverk, N. Atlasy, A. Bujko, S. Yaqub, R. Horneland, O. Øyen, E.M. Aandahl, K.E.A. Lundin, H.G. Stunnenberg, et al. 2018. Transcriptional profiling reveals monocyte-related macrophages phenotypically resembling DC in human intestine. *Mucosal Immunol.* 11: 1512–1523. https://doi.org/10.1038/s41385-018-0060-1

Risnes, L.F., A. Christophersen, S. Dahal-Koirala, R.S. Neumann, G.K. Sandve, V.K. Sarna, K.E. Lundin, S.W. Qiao, and L.M. Sollid. 2018. Disease-driving CD4+ T cell clonotypes persist for decades in celiac disease. *J. Clin. Invest.* 128:2642–2650. https://doi.org/10.1172/JCI98819

Ruiz, P., H. Takahashi, V. Delacruz, E. Island, G. Selvaggi, S. Nishida, J. Moon, L. Smith, T. Asaoka, D. Levi, et al. 2010. International grading scheme for acute cellular rejection in small-bowel transplantation: single-center experience. *Transplant. Proc.* 42:47–53. https://doi.org/10.1016/j.transproceed.2009.12.026

Russell, G.J., C.M. Parker, A. Sood, E. Mizoguchi, E.C. Ebert, A.K. Bhan, and M.B. Brenner. 1996. p126 (CDw101), a costimulatory molecule preferentially expressed on mucosal T lymphocytes. *J. Immunol.* 157: 3366–3374.

Sadee, C., M. Pietrzak, M. Seweryn, and G. Rempala. 2017. divo: Tools for analysis of diversity and similarity in biological systems. Available at: https://rdrr.io/cran/divo/ (accessed July 17, 2018).

Schenkel, J.M., K.A. Fraser, L.K. Beura, K.E. Pauken, V. Vezys, and D. Masopust. 2014. T cell memory. Resident memory CD8 T cells trigger protective innate and adaptive immune responses. *Science.* 346:98–101. https://doi.org/10.1126/science.1254536

Schön, M.P., A. Arya, E.A. Murphy, C.M. Adams, U.G. Strauch, W.W. Agace, J. Marsal, J.P. Donohue, H. Her, D.R. Beier, et al. 1999. Mucosal T lymphocyte numbers are selectively reduced in integrin alpha E (CD103)-deficient mice. *J. Immunol.* 162:6641–6649.

Schwartzkopff, S., S. Woyciechowski, U. Aichele, T. Flecken, N. Zhang, R. Thimme, and H. Pircher. 2015. TGF-β downregulates KLRG1 expression in mouse and human CD8(+) T cells. *Eur. J. Immunol.* 45:2212–2217. https://doi.org/10.1002/eji.201545634

Sheridan, B.S., Q.M. Pham, Y.T. Lee, L.S. Cauley, L. Puddington, and L. Lefrançois. 2014. Oral infection drives a distinct population of intestinal resident memory CD8(+) T cells with enhanced protective function. *Immunity.* 40:747–757. https://doi.org/10.1016/j.immuni.2014.03.007

Snyder, M.E., M.O. Finlayson, T.J. Connors, P. Dogra, T. Senda, E. Bush, D. Carpenter, C. Marboe, L. Benvenuto, L. Shah, et al. 2019. Generation and persistence of human tissue-resident memory T cells in lung transplantation. *Sci. Immunol.* 4:eaav5581. https://doi.org/10.1126/sciimmunol.aav5581

Steinert, E.M., J.M. Schenkel, K.A. Fraser, L.K. Beura, L.S. Manlove, B.Z. Igyártó, P.J. Southern, and D. Masopust. 2015. Quantifying Memory CD8 T Cells Reveals Regionalization of Immunosurveillance. *Cell.* 161: 737–749. https://doi.org/10.1016/j.cell.2015.03.031

Tao, L., and T.A. Reese. 2017. Making Mouse Models That Reflect Human Immune Responses. *Trends Immunol.* 38:181–193. https://doi.org/10.1016/j.it.2016.12.007

Thome, J.J., N. Yudanin, Y. Ohmura, M. Kubota, B. Grinshpun, T. Sathaliyawala, T. Kato, H. Lerner, Y. Shen, and D.L. Farber. 2014. Spatial map of human T cell compartmentalization and maintenance over decades of life. *Cell.* 159:814–828. https://doi.org/10.1016/j.cell.2014.10.026

Thompson, E.A., J.S. Mitchell, L.K. Beura, D.J. Torres, P. Mrass, M.J. Pierson, J.L. Cannon, D. Masopust, B.T. Fife, and V. Vezys. 2019. Interstitial Migration of CD8αβ T Cells in the Small Intestine Is Dynamic and Is Dictated by Environmental Cues. *Cell Reports.* 26:2859–2867.e4. https://doi.org/10.1016/j.celrep.2019.02.034

Vander Heiden, J.A., G. Yaari, M. Uduman, J.N. Stern, K.C. O'Connor, D.A. Hafler, F. Vigneault, and S.H. Kleinstein. 2014. pRESTO: a toolkit for processing high-throughput sequencing raw reads of lymphocyte receptor repertoires. *Bioinformatics.* 30:1930–1932. https://doi.org/10.1093/bioinformatics/btu138

Watanabe, R., A. Gehad, C. Yang, L.L. Scott, J.E. Teague, C. Schlapbach, C.P. Elco, V. Huang, T.R. Matos, T.S. Kupper, and R.A. Clark. 2015. Human skin is protected by four functionally and phenotypically discrete populations of resident and recirculating memory T cells. *Sci. Transl. Med.* 7:279ra39. https://doi.org/10.1126/scitranslmed.3010302

Wickham, H. 2009. *ggplot2: Elegant Graphics for Data Analysis*, vol. VIII. Springer-Verlag, New York, 213 pp. https://doi.org/10.1007/978-0-387-98141-3

Zuber, J., B. Shonts, S.P. Lau, A. Obradovic, J. Fu, S. Yang, M. Lambert, S. Coley, J. Weiner, J. Thome, et al. 2016. Bidirectional intragraft alloreactivity drives the repopulation of human intestinal allografts and correlates with clinical outcome. *Sci. Immunol.* 1:eaah3732. https://doi.org/10.1126/sciimmunol.aah3732